Studies on Effects of Periodic Wake Passing upon a Blade Leading Edge Separation Bubble*

(Suppresion of Separation Bubble Due to Wake Passing)

Ken-ichi FUNAZAKI**, Kazutoyo YAMADA** and Yoshiki KATO***

This paper describes an experimental investigation on aerodynamic interaction between incoming periodic wakes from moving bars and separation bubble on a scaled leading edge model. Numerical simulations are also attempted to grasp an idea how the incoming wakes interact with the separation bubble. The model, which consists of a semi-circular leading edge and two flat-plates, is used to simulate the flow field around a compressor or a turbine blade. Cylindrical bars of the wake generator produce the periodic wakes in front of the test model. The study aims at enriching the knowledge on how and to what extent the periodic wake passing suppresses the leading edge separation bubble. Special attention is paid to emergence of wake-induced turbulent spots and subsequent calmed regions. Hot-wire probe measurements are executed under five different flow conditions to examine effects of Reynolds number, Strouhal number, direction of the bar movement and incidence of the test model against the incoming flow. The measurements reveal that the wake moving over the separation bubble does not directly suppress the separation bubble. Instead, wake-induced turbulence spots and the subsequent calmed regions have dominant impacts on the separation bubble suppression for the all test cases.

Key Words: Separation Bubble, Wake Passing, Blade Leading Edge, Experiment

1. Introduction

A great number of studies have been made to investigate the interaction between periodically incoming wakes and separation bubble on low-pressure compressor or turbine blades and vanes, aiming at the acquisition of detailed information on the behaviors of the separation bubble under the influence of the wake passing. For example, Halstead et al.[1),(2)] comprehensively reported on ensemble-averaged quasi-wall shear stress on compressor or turbine blades to elucidate the interaction between upstream wakes-the blade boundary layer using test rigs for compressors and turbines. Cumptsy et al.[3)] investigated wake-affected boundary layers containing separation bubble on a compressor cascade. Schulte and Hodson[4)], Kaszeta, Simon and Ashpis[5)], examined wake-separation bubble interaction using linear turbine cascades and moving bars, each of which intended to clarify favorable effects of the wake passing upon the separation bubble as one of the approaches to reduce profile loss.

In contrast to those accumulating knowledge concerning the separation bubble on the blade suction surface, less information is available on the interaction between the incoming wakes and leading edge separation bubble on a compressor or a turbine blade. Except for a pioneering effort done by Paxson and Mayle[6)], few attention has been paid to the leading edge flow fields with separation bubble. Recently, Brear et al.[7)] examined flow separation occurring just behind the blade leading edge on the pressure surface of LP turbine cascade subjected to the periodic wakes from the moving bars. Flow visualizations and aerodynamic loss measurements were made in their study, showing that the shear layer was found to be slightly affected by the wake passing or increased free-stream turbulence. Funazaki and Kato[8)], using a simple scaled leading edge model of a compressor blade and the moving bar mechanism, executed detailed measurements of the separated boundary layer on the test model affected by the periodic wake passing. Similarly, a simplified flat-plate model experiment was made by Ottavy et al.[9)], followed by Chun

* Received 26th December, 2003 (No. 03-4213)

** Department of Mechanical Engineering, Iwate University, 3–5 Ueda 4, Morioka 020–8551, Japan.
E-mail: funazaki@iwate-u.ac.jp

*** Ishikawajima-Harima Heavy Industries Co., Shin-Nakaharamachi 1, Isogo, Yokohama 235–8501, Japan

and Sung[10].

The present study is an extended version of the previous study by Funazaki and Kato[8] using almost the same test facility, aiming at the clarification about how and to what extent the periodic wake passing suppresses the leading edge separation bubble occurring near the leading edge of the test model under various flow conditions, such as wake-passing Strouhal number, inlet Reynolds number and incident of the model. Special attention is paid to the emergence of wake-induced turbulence spots followed by calmed region. These flow events were already reported by Funazaki and Kato[8] with less quantitative discussion, though. Time-accurate numerical simulation is also made using a RANS (Reynolds-Averaged Navier-Stokes equations) solver with Wilcox k-ω turbulence model to provide an idea on how the incoming periodic wakes interact with the separation bubble.

2. Nomenclature

d : bar diameter
f_{bp} : bar-passing frequency ($= U_b/p$)
i : incidence
N : number of data segments for ensemble-averaging
P : bar pitch ($= 0.317\,5$ m)
R : radius of the leading edge of the test model
Re : Reynolds number ($= U_{in}R/\upsilon$)
t : time
T : bar-passing period ($= p/U_b$)
T^* : time length of data segment for ensemble averaging
Tu^* : ensemble-averaged turbulence intensity
U_b : bar speed
U_{in} : inlet velocity
$U_{\max}$: maximum velocity attained near the surface
U_{ref} : reference velocity measured at $y = 50$ mm
u_k, u^*, $\bar{u}$: raw velocity data, ensemble-averaged velocity and time-averaged velocity
x_s : distance along the surface from the leading edge
Y : vertical distance from the center line of the test model
y : vertical distance from the test model surface
$y_{\max}$: height where the maximum velocity $U_{\max}$ appeared
υ : kinematic viscosity
δ_1^*, δ_2^* : ensemble-averaged displacement and momentum thickness

3. Experimental Apparatus

3.1 Test facility

As mentioned earlier, test facility used in this study was almost the same as that in the previous study[8]. Figure 1 shows the experimental setup, including the detail of the wake generator. The wake generator, which was attached to the exit of the contraction nozzle, consisted of two long timing belts, four geared pulleys and stainless-steel bars. Both ends of the bars with 6 mm diameter were tightly fixed to the belts as shown in Fig. 1 using connecting profiles glued on both of the belts. The pitch of the profiles was 63.5 mm and the profile number was 50. The induction motor drove the belts in such a way that the bars crossed the main flow at a speed ranging from 4.5 m/s to 7.5 m/s and the direction of the bar movement was reversible. The distance between the upstream and downstream loci of the bars was about 300 mm.

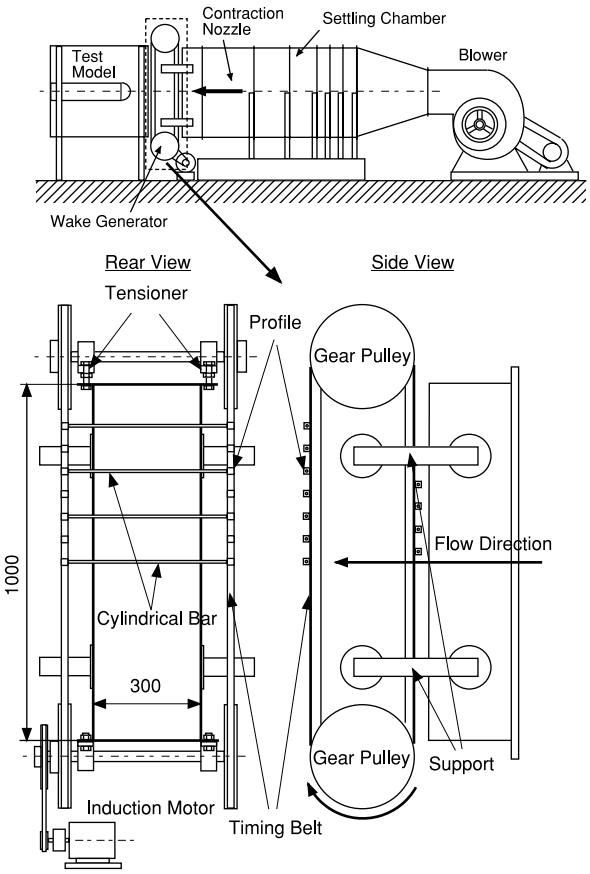

Fig. 1 Test apparatus with wake generator

Figure 2 depicts the test model in the test duct. The model, with a semi-circular leading edge of 100 mm radius ($= R$) and two flat plates, was 900 mm long and 280 mm wide. Two thin fences were attached to the test model surface near the both side walls of the duct to minimize sidewall contamination. The model was distanced by 245 mm from the downstream locus of the moving bars. A Pitot tube monitored the inlet velocity in front of the test section. The test model could be tilted to change incidence against the inlet flow.

3.2 Test conditions

Table 1 is the test conditions of this study. Test Case 1 was a baseline experiment, where the inlet velocity U_{in} was 10 m/s and the bars moved upwards just in front of the model at a speed of 6 m/s. Reynolds number Re based on

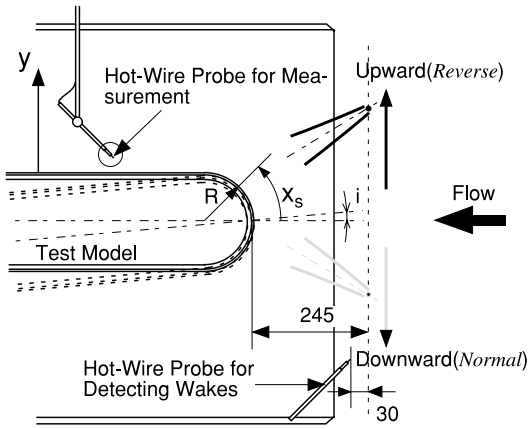

Fig. 2 Test model and two hot-wire probes

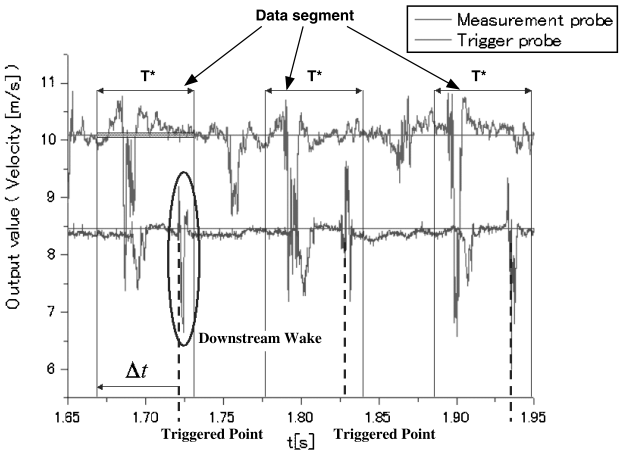

Fig. 3 Test model and two hot-wire probes

Table 1 Test condition

Test Case	Bar Movement	U_{in} [m/s]	U_b [m/s]	Re x 10^{-4}	St	i [deg]
1	Upward	10	6	0.67	0.185	0
2	Downward	10	6	0.67	0.185	0
3	Upward	10	7.5	0.67	0.231	0
4	Upward	7.5	4.5	0.50	0.185	0
5	Upward	10	6	0.67	0.185	5

the radius of the model leading edge and the inlet velocity was 6.7×10^4. Test Case 2 aimed to see whether any difference could be identified in comparison with the results of Test Case 1 when the wakes were generated from the bars moving *downwards*. Test Case 3, where the bar speed was increased by 25% from the baseline experiment, was for examining the effect of wake-passing frequency or Strouhal number. Caution was necessary in interpretation of the results of Test Case 3 because the wake characteristics changed due to the change in relative inlet velocity against the bar. Reynolds number effects were investigated in Test Case 4, where the bar speed was decreased so as to keep the Strouhal number the same as that of Test Case 1. In Test Case 5 the model was tilted as shown in Fig. 2 to change the incidence from 0° to 5°, resulting in larger separation bubble in this case.

The measurement region extended from $x_s/R = 0.96$ (distanced by 55° from the center line) to $x_s/R = 4.57$ in the streamwise direction and from $y/R = 0.3\times10^{-2}$ to $y/R = 0.5$ in the vertical direction.

3.3 Data acquisition

As can be easily understood from Fig. 1, the bars in the wake generator passed across the main flow twice in one revolution of the belts at the different streamwise positions. This inevitably resulted in two different types of the wakes, i.e., 'upstream wakes' generated at the far upstream of the test model and 'downstream wakes' near the model. Since this study intended to investigate only the effect of the 'downstream wakes', great care had to be paid to the selection of the bar pitch and bar count in order to make the measurement window being undisturbed by the 'upstream wakes' as long as possible. Several trials finally determined that three bars with the pitch (p) of 317.5 mm on the belts sufficed the above-mentioned requirement.

Figure 2 also shows two miniature hot-wire probes (Dantec 55P11). The probe locating above the model was to measure the flow field around the test model and called *measurement probe*. The other probe, called *trigger probe*, was placed in the lower part of the test duct to detect the arrival of the downstream wakes from the bars. Both probes were connected to a CTA unit (Dantec Streamline) that was fully controlled by a PC. Outputs of the hot-wire probes were compensated to the main flow temperature fluctuation. They were then simultaneously acquired and converted from analog to digital by a built-in A/D converter, the digitized data being finally stored into the PC. Note that for one measurement point the system captured velocity data of 2^{16} samples with the sampling frequency of 5 kHz, where this relatively low sampling frequency was employed for maximizing the bar wake count in one velocity record.

3.4 Ensemble-average quantities

Figure 3 shows an example of the velocity signals acquired by the two different probes, indicating the appearance of the two different types of wakes. Periodic velocity data segments of time length T^* were carefully extracted from the signal of the measurement probe so that the upstream wake was not included in each of the segments. In this case, the downstream wake detected by the trigger probe was used to determine the starting point of each of the data segments.

Since the sampling frequency was 5 kHz and one measurement lasted for about 13 sec ($=2^{16}/5\,000$), the total number of the revolutions of the timing belts during the one measurement was at least 18 even for the slowest belt speed case (Test Case 3). One revolution of the belts generated 3 wakes, meaning that more than 50 signals of the downstream wakes passing over the boundary layer were available for each of the realizations. Ensemble-averaged velocity u^* was then calculated from the extracted 50 data

segments as follows;

$$u^*(x,y;t)=\frac{1}{N}\sum_{k=1}^{N}u_k(x,y;t),\ N=50 \tag{1}$$

The count of the segments for this ensemble-averaging was rather small in comparison with those commonly used in any other studies, however, as discussed later, $N=50$ was found to be a satisfying count, at least in the present case.

Ensemble-averaged velocity fluctuation $\Delta u_k^*(x,y;t)$ was also evaluated by

$$\Delta u_k^*(x,y;t)=u_k^*(x,y;t)-\bar{u}(x,y), \tag{2}$$

where $\bar{u}(x,y)$ was time-averaged velocity calculated by

$$\bar{u}(x,y)=\frac{1}{T}\int_{t_0}^{t_0+T}u^*(x,y;t)dt. \tag{3}$$

Ensemble-averaged turbulence intensity was also defined as,

$$Tu^*(x,y;t)=\sqrt{\frac{1}{N-1}\sum_{k=1}^{N}\Delta u_k^{*2}}\Big/U_{\mathrm{ref}}, \tag{4}$$

where U_{ref} was a reference velocity, and in this case the time-averaged velocity obtained at the upper limit of the measurement region, i.e., $y/R=0.5$, was adopted.

Boundary layer integral parameters were then calculated from the following expressions using the ensemble-averaged velocity;

$$\delta_1^*(x;t)=\int_0^{y_{\max(x;t)}}\left(1-\frac{u^*(x;t)}{U_{\max}(x,t)}\right)dy, \tag{5}$$

$$\delta_2^*(x;t)=\int_0^{y_{\max(x;t)}}\frac{u^*(x,t)}{U_{\max}(x;t)}\left(1-\frac{u^*(x;t)}{U_{\max}(x;t)}\right)dy, \tag{6}$$

where δ_1^* and δ_2^* were ensemble-averaged displacement thickness and momentum thickness, respectively. Note that $y_{\max}(x,t)$ was the location where the velocity reached the maximum $U_{\max}(x,t)$ in the vicinity of the test model surface and regarded as the boundary layer thickness in this study.

3.5 Uncertainty analysis

Since the calibration curve of a 4-th order polynomial matched the velocity data measured with a pneumatic probe quite well, a major contributor to the uncertainty in the hot-wire measurements was the error in the pneumatic probe measurement. This error, mainly depending on the accuracy of the pressure transducer used, was estimated to be about ±0.6 m/s.

Besides, the convergence rate of the ensemble-averaging surely had a serious impact on the uncertainty of the resultant velocity. Figure 4 shows an example of the convergence histories of the ensemble-averaging with the increase of the number of the data segment N, where the experimental raw data at $x_s/R=1.695$ and $y/R=0.05$ was used. It seems that the ensemble-averaged velocity calculated from more than 50 velocity segments almost reached convergence, with the average residual less than 0.05 m/s.

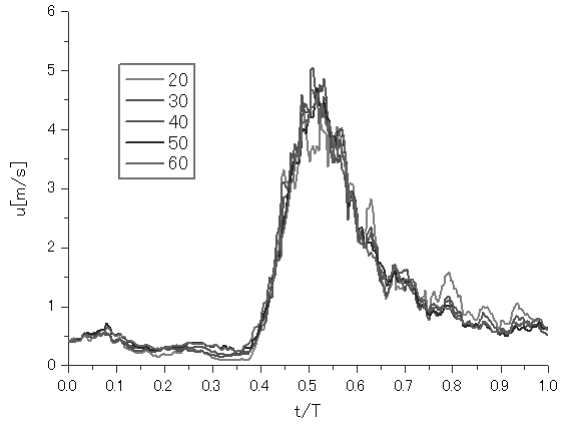

Fig. 4 Example of convergence histories of the ensemble-averaged velocity

Single hot-wire probes cannot detect reversed flow without any manipulations, so that the present measurements inevitably suffered from the under- or overestimations of the boundary layer integral parameters given by Eqs. (5) and (6). Detailed investigations revealed that in the no wake case, which was the worst case, the displacement thickness was underestimated by 7% and the momentum thicknesses were overestimated by 50%, respectively, at the position where the reversed flow became active most.

4. Numerical Scheme

4.1 Flow solver and computing system

Time-accurate three-dimensional flow simulation was performed by solving the Reynolds-averaged Navier-Stokes equations using an unfactored implicit upwind relaxation scheme with inner iterations. The numerical method used is outlined in the following. The governing equations were discretized in space using a cell-centered finite volume formulation and in time using the Euler implicit method. The inviscid fluxes were evaluated by a high-resolution upwind scheme based on a TVD formulation developed by Furukawa et al.[11], where a Roe's approximate Riemann solver of Chakravarthy[12] and a third-order accurate MUSCL approach of Anderson et al.[13] with the Van Albada limiter were implemented. The viscous fluxes were evaluated in a central-difference manner. The k–ω turbulence model proposed by Wilcox[14] was employed to estimate the eddy viscosity. Simultaneous equations linearized in time were solved by a point Gauss-Seidel relaxation method using no approximate factorization. To obtain a time-accurate solution, inner iterations, so-called Newton iterations were introduced at each time step. The scheme was kept second-order accurate in time by applying the three-point-backward difference approximation to the temporal derivative. For the unsteady flow simulations presented in this paper, more than 20 inner iterations were made at each time step, and a nondimen-

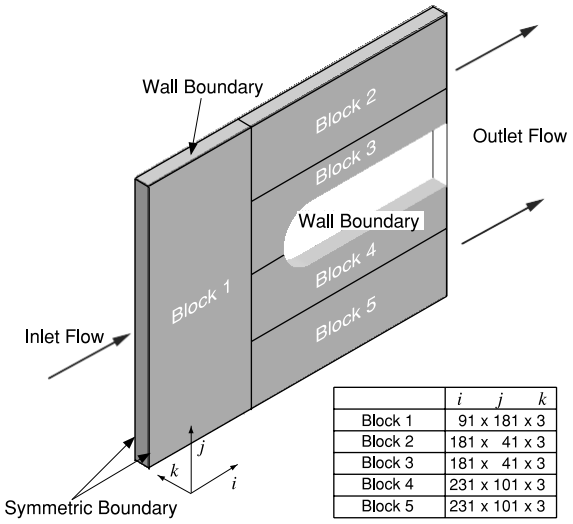

	i	j	k
Block 1	91	181	3
Block 2	181	41	3
Block 3	181	41	3
Block 4	231	101	3
Block 5	231	101	3

Fig. 5 Multi-block grid system used in the simulation

sional time step size normalized by the leading edge radius of the model and a speed of sound at the inlet was set to 0.2.

The computing system used was a PC-cluster with 8 nodes, each of which contained one Intel Xeon processor of 2.4 GHz speed and 6 MB main memory. Gigabit and megabit network system was constructed in the PC-cluster, where the gigabit system exchanged the numerical data and the megabit system was for network operation such as NFS.

4.2 Grid system and boundary conditions

The code was parallelized using MPI (Message Passing Interface), and a five-block grid system along with the information on boundary conditions are shown in Fig. 5. The detail of each of the blocks is also listed in Fig. 5. The spanwise length of the system was relatively short because the flow field concerned was almost two-dimensional. To emulate the experiment, equally spaced wake profiles that were experimentally determined were specified on the inlet plane. These wake profiles slid along the inlet plane at the bar speed U_b. Other boundary conditions such as inlet velocity or inlet Reynolds number were taken from the experiments.

5. Results

5.1 Steady-state flow measurements

Figure 6 displays velocity profiles of the separated boundary layer measured at several streamwise stations without the bar wake influence. The velocity at any streamwise position was normalized by its reference velocity U_{ref}. The separation occurred almost at the junction of the semi-circular leading edge and the flat plate, because of the difference in curvature. The thickness of the separation bubble was found to be about 2.0 mm (0.02 when normalized by R). Comparing these profiles with Horton's mean reattachment profile[15], it was found that

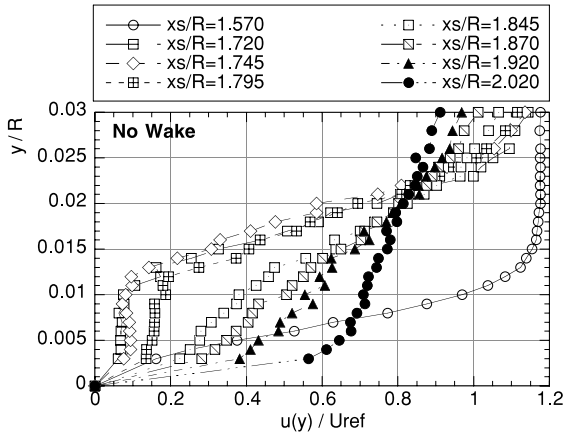

Fig. 6 Velocity profiles of the separated boundary layer for no wake condition

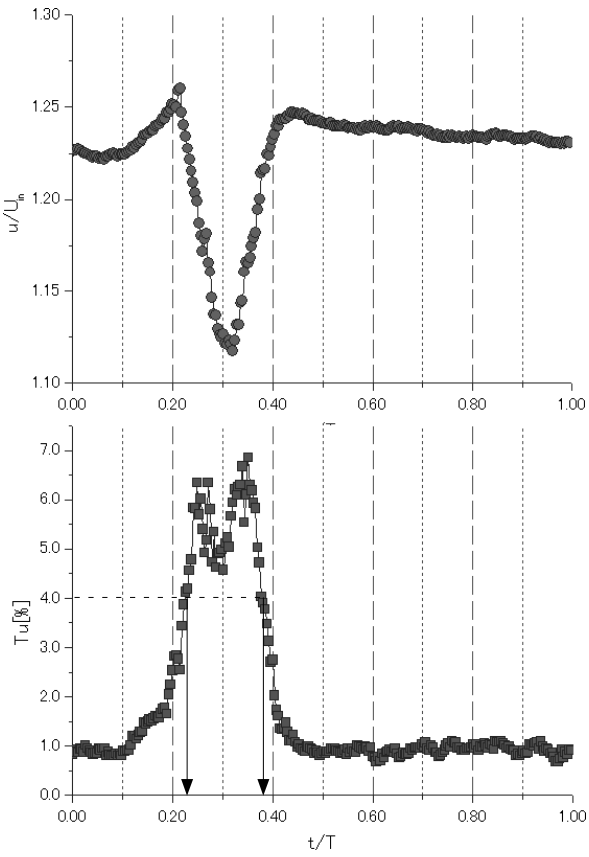

Fig. 7 Velocity (upper) and turbulence intensity (lower) profiles in the wake generated by the moving bar of 6 mm diameter (location: $x/R = 1.308$, $y/R = 0.5$)

the reattachment point located around $x_s/R = 1.87$.

5.2 Wake profile

Figure 7 shows ensemble-averaged velocity and turbulence intensity of the moving-bar wake of Test Case 1. They were obtained by the hot-wire probe located near the leading edge of the test model (x_s/R = 1.308 and $y/R = 0.5$) during one wake passing period. The data shown here was normalized by the inlet velocity U_{in}. Despite a flow acceleration near the leading edge, the veloc-

ity deficit of the wake retained about 0.1 U_{in} and the maximum wake turbulence was about 7%. Two peaks in the turbulence intensity due to the shear layers inside the wake were clearly observed. It follows from this figure that the wake with more than 4% turbulence intensity, which could be regarded as an effective turbulence intensity[16], lasted for about 15% of the bar passing period.

5.3 Emergence of turbulence spots and calmed region

5.3.1 Discussion using boundary layer parameters Figure 8 shows contours of the ensemble-averaged displacement and momentum thicknesses on the x_s-time plane for Test Case 1 (the bar moving upwards). Also shown in this figure are five lines on each of the contours, which represent traces of the fluid particles moving at 100%, 90%, 50% and 30% speed of $\overline{U_{\mathrm{ref}}}$, streamwisely averaged velocity of U_{ref} over the measurement region. In Fig. 8, the wide zone of large displacement thickness appeared from $x_s/R = 1.6$ to $x_s/R = 1.8$, which was attributed to the existence of the separation bubble.

Before going into detail of the wake interaction with the separation bubble, a brief comment seems necessary on how the positions of those lines were determined. Because of its low velocity and consequently large value of $y_{\max}$, the incoming wake tended to leave its footprint in terms of a strip of relatively large displacement thickness. Taking advantage of this tendency, the wake path on the contour of the displacement thickness was easily spotted as the 100% speed traces of the fluid particle as shown in the left contours of Fig. 8. A triangle zone of large value of the displacement thickness, denoted T.S. in this figure, appeared behind the wake path. Under the assumption that this zone was a consequence of wake-induced turbulence spots growing towards the downstream, particle traces of 90% and 50% speed were chosen to sketch out the zone, where the starting points of each of the traces were fixed on the same position. Note that 90% and 50% speeds are regarded as the propagation velocities of front and rear parts of a turbulent spot, respectively. A trace of 30% speed, which represents the rear end of calmed region[17], also started from the same point as the 90% and 50% traces. From the fact that 90% and 50% speed traces were smoothly fitted to the triangle-shaped zone of large displacement thickness in Fig. 8, it can be concluded that the triangle-shaped zone was the consequence of wake-induced turbulence spots. It turned out that the procedure to determine the positions of the traces worked quite well in Test Case 1, and as will be shown in the following, the same approach was actually found to be valid among the other test cases, except for Test Case 2.

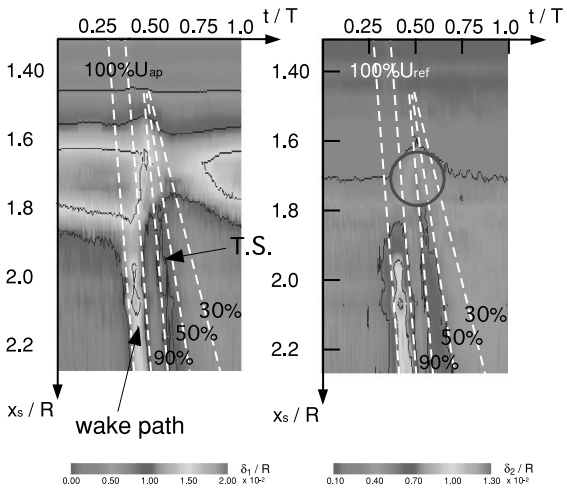

Fig. 8 Ensemble-averaged displacement and momentum thicknesses on x_s-time planes for Test case 1 (left: Displacement thickess/right: Momentum Thickness)

The same traces were used in the momentum thickness contours as in the displacement thickness contours without any modifications. Again, the fluid particle traces agreed with the profiles of the regions with relatively high value which were seemingly associated with the wake as well as turbulent spots. Besides, the momentum thickness data spotted an area marked by the circle. This area almost laid itself underneath the path enclosed by 90% and 50% speed traces. Since any increase in momentum thickness usually means the progress of boundary layer transition, the appearance of this area also supports the conclusion here that the incoming wake induced turbulent spots that strongly affected the separation bubble. The important point here was that the spots in this case abruptly emerged almost at or rather upstream of the separation point. This was probably because of the adverse pressure gradient observed by Funazaki et al.[18] or the change in curvature as a catalyst of the transition, although much remains to be studied in the future. As discussed in the following, onset points of the turbulent spots, which were determined by the curve-fitting approach, exhibited a slight dependency to the flow conditions such as Reynolds number or Strouhal number.

5.3.2 Discussion using velocity fluctuation and turbulence intensity Figure 9 shows a composite representation of velocity fluctuation, turbulence intensity and velocity profile in x_s, y and time domain for Test Case 1. This figure clearly demonstrates the existence of the incoming wake and the appearance of the induced turbulence spots behind the wake in terms of the decelerated zone, where the deceleration was measured from the local averaged velocity (see Eq. (2)). High turbulence intensity zone, which contained more than 14% local turbulence intensity and was roughly hatched in this figure, started to shrink after the passage of those decelerated zone. Since the high turbulence intensity originated mostly from unstable shear layer of the separation bubble, this shrinkage indicated that the wake passage surely suppressed the sep-

aration bubble for relatively long period.

5.4 Effects of the bar-moving direction and strouhal number

5.4.1 Test Case 1 (bar moving upwards) In Test Case 1, baseline case, the wide zone having large displacement thickness almost disappeared while the incoming wake swept over the test model, then recovered afterwards. This indicates that the leading edge separation bubble experienced temporal suppression because of the passage of the incoming wake. Important features to be mentioned were found in Figs. 8 and 9. The observation shows that the separation bubble with large displacement thickness remained almost unaffected even just beneath the wake path. It seems that the wake passage itself did not make an explicit contribution to the suppression of the separation bubble in this case. In contrast, the reduction of the displacement thickness indicates that the wake-induced turbulence spots and the following calmed region surely suppressed the separation bubble. A similar conclusion can be drawn from the observations of the ensemble-averaged velocity in Fig. 10, where the low speed zone associated with the separation bubble became small when the turbulent spots, then the calmed region passed over the separation bubble.

The turbulent spots, whose origins were identifiable from the intersection of the traces, slightly lagged behind the wake passage in this case. The footprints of the wake passage could be found on the near-wall plane ($y/R = 0.005$) as well as on the plane with its height from the wall almost same as that of the separation bubble ($y/R = 0.020$). On the plane of $y/R = 0.005$ in Fig. 10, the 100% speed traces could be shifted in the right direction from the original position of Fig. 8 by some distance so that the traces agreed with the wake passage footprint at the location denoted by the circle A. Since this shifting brought about the attachment of the 100% traces to the other traces, it can be stated that the turbulence spots actually emerged just after the wake passage near the surface. In other words, the upstream wake was mainly responsible for the generation of the turbulent spots. The shifted distance of the traces corresponded to about 7% of the wake passing period, meaning that the wake suffered from large deformation due to the blockage effect of the test model and/or lagged behind the free-stream within the boundary layer.

Circle B in Fig. 10 shows that the separation bubble did not fully recover from the influence of the upstream wake passing even after the passage of the turbulent spots and the calmed region. One possible reasoning on this phenomenon is "negative-jet effect" of the upstream wake interacting with the leading edge of the test model.

Figure 11 shows a snapshot of the numerical simulations showing the interaction of the wake with the sepa-

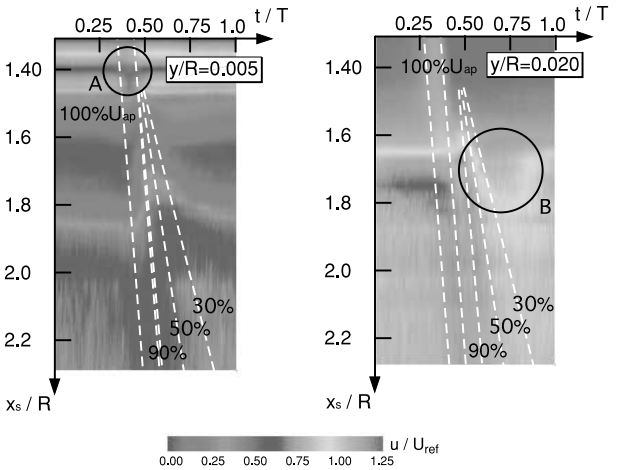

Fig. 10 Ensemble-averaged velocity on x_s-time planes for Test case 1 (left: $y/R = 0.005$/right: $y/R = 0.020$)

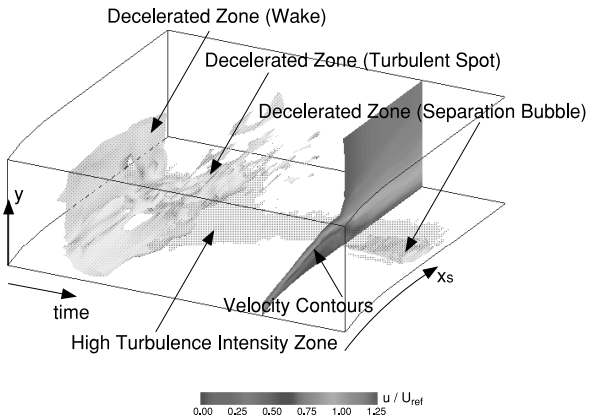

Fig. 9 Composite 3D representation showing velocity fluctuation, turbulence intensity and velocity profile for Test case 1

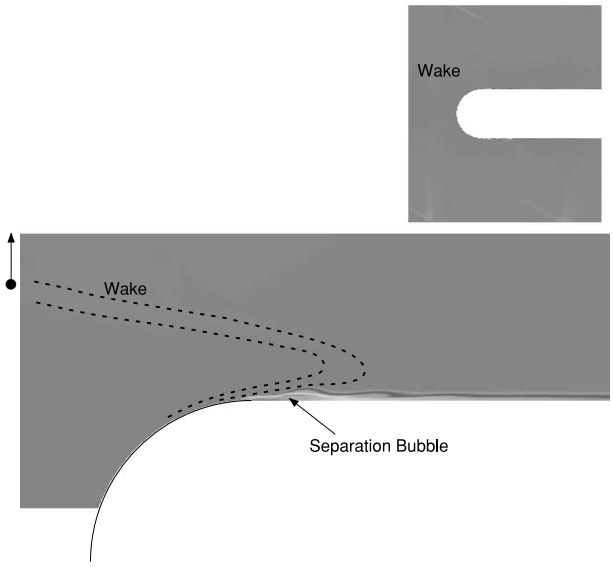

Fig. 11 Snapshot of calculated wake interaction with the separation bubble

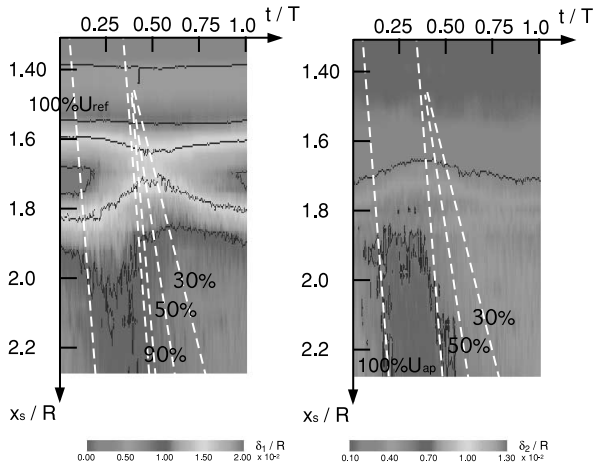

Fig. 12 Ensemble-averaged displacement and momentum thicknesses on x_s-time planes for Test case 2 (left: Displacement thickess/right: Momentum Thickness)

ration bubble on the test model. The predicted separation bubble was found to exhibit unsteady feature with periodic vortex shedding. Although the code lacked ability to predict the transitional behavior of the shear layer of the separation bubble, the size of the bubble seemed to be reasonably predicted. Figure 11 also indicates that the wake deformed around the leading edge, however, it seems that the wake passage had almost no impact on the separation bubble but just moved over it, which matches the experimental observation shown in Fig. 9.

5.4.2 Test Case 2 (bar moving downwards) Figure 12 depicts contours of the ensemble-averaged displacement and momentum thicknesses on the x_s-time plane for Test Case 2 (the bar moving downwards). Clearly, the wake duration in Test Case 2 was much longer than that of Test Case 1. The separation bubble was gradually shrunk but not fully extinguished while the wake passed over it, which was in contrast to Test Case 1. Rather surprisingly, wake-induced turbulence spots and calmed region were not clearly seen in this figure, although the separation bubble was still suppressed for some time period. The appearance of the larger wake duration in the *normal* moving case was already reported by Funazaki et al.[16], which was also due to "negative-jet effect". Figure 13 shows the ensemble-averaged velocities on the y-time planes for Test Case 1 (left) and Test Case 2 (right), again emphasizing the difference between the two cases in terms of bar-wake interaction with the separation bubble. The data in this figure was acquired at $x_s/R = 1.745$ where the separation bubble reached its maximum height in no wake case as shown in Fig. 5. The left contours in Fig. 13 clearly depict that turbulent spots appeared behind the wake, penetrating the free-stream. Underneath the turbulent spots, the separation bubble, which was usually characterized by very low speed zone, was temporarily diminished. On the contrary, the wake in Test Case 2 was rather vague and did not seem to be accompanied by any turbulence spots. Furthermore, the separation bubble in this case was not completely extinguished, while it experienced the wake passage and its influence for longer time than in Test Case 1. At this moment the reason for this distinct difference has not been clarified yet.

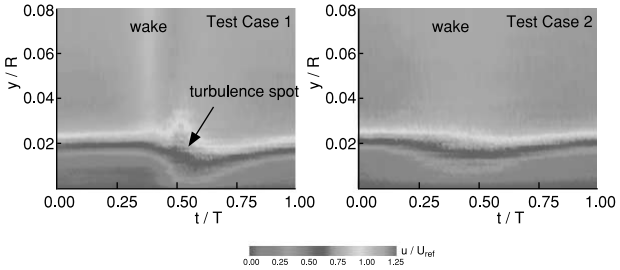

Fig. 13 Bar wakes interacting with the separation bubble on y-time planes of ensemble-averaged velocity measured at $x_s/R = 1.745$ (left: Test Case 1/right: Test Case 2)

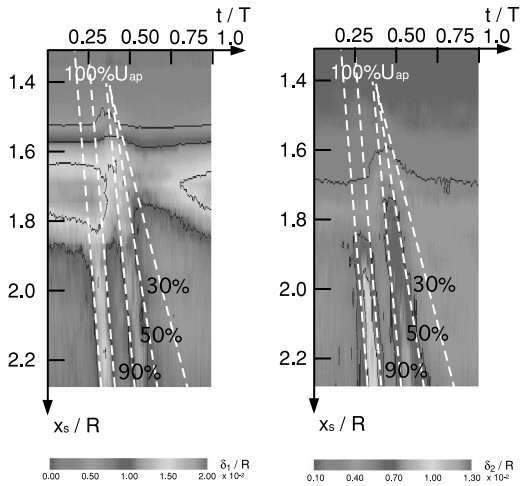

Fig. 14 Ensemble-averaged displacement and momentum thicknesses on x_s-time planes for Test case 3 (left: Displacement thickess/right: Momentum Thickness)

5.4.3 Test Case 3 (higher Strouhal number) Figure 14 is the results of Test Case 3; higher Strouhal number case. Since the Strouhal number increased only by 25% of the original value, overall views of the displacement and momentum thickness contours quite resembled those of Test Case 1. However, the onset of the wake-induced turbulence spots, which was equivalent to the origin of the spots in this study, took place a little earlier than in Test Case 1, probably because of enhanced wake turbulence.

5.5 Effects of the mean flow conditions

Figure 15 shows two contours of the wake-affected displacement thickness on x_s-time diagrams obtained for Test Case 4 and Test Case 5. Since the Reynolds number was reduced by 25% in Test Case 4 or the incidence was increased from 0 deg to 5 deg, the separation bub-

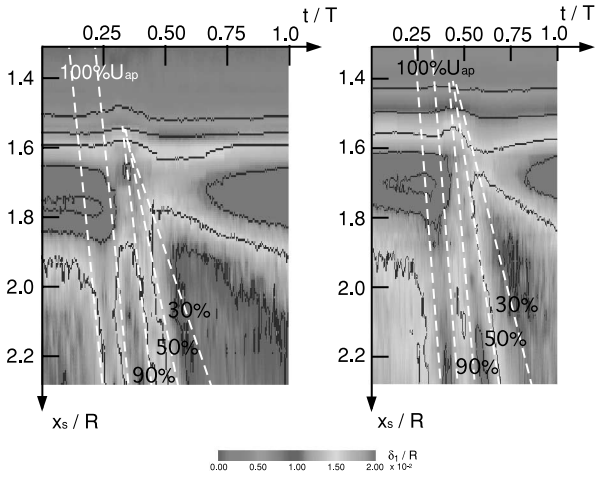

Fig. 15 Ensemble-averaged displacement on x_s-time planes (left: Test Case 4/right: Test Case 5)

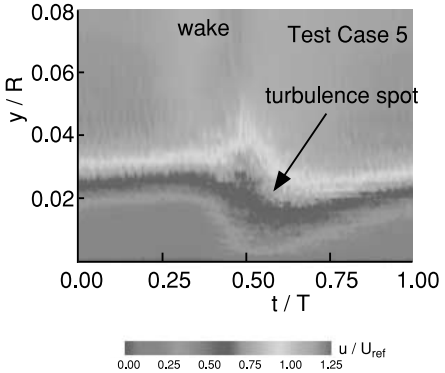

Fig. 16 Bar wakes interacting with the separation bubble on y-time planes of ensemble-averaged velocity measured at $x_s/R = 1.745$ (Test Case 5)

ble for each of the test cases became considerably larger than Test case 1, which could be confirmed by looking at the extent of the high displacement thickness zone as well as at the peak value within the zone. Wake-induced turbulence spots clearly appeared, slowly being lagged from the wake in both test cases. The onset of the turbulent spots in Test Case 4 (left of Fig. 15) was found around $x_s/R = 1.6$, while $x_s/R = 1.5$ for Test case 1. This delay could be attributed to the effect of the reduced Reynolds number. On the other hand, the onset of the wake-induced turbulence spots in Test case 5 started earlier than in Test case 1. This was probably because the surface length from the aerodynamic stagnation point to a point concerned was in effect elongated by about 0.09 in x_s/R. Figure 16, ensemble-averaged velocity measured at $x_s/R = 1.745$, indicates that wake-induced turbulent spots appeared behind the wake, abruptly diminishing the separation bubble of very low speed zone. Thereafter, the separation bubble started to recover in a gradual manner.

6. Conclusions

This study dealt with hot-wire probe measurements of separated boundary layer around the leading edge of the blunt test model which was subjected to periodic wake passing. The focus of this study was on the suppression of the separation bubble under the various flow conditions, i.e., the two directions of the wake-generating bar movement, wake-passing Strouhal number, Reynolds number and incidence. The findings in this study can be summarized as follows.

(1) When the wake-generating bar moved upwards, the emergence of wake-induced turbulence spot, followed by the resultant calmed region, were identified behind the wake in the contours of the time-resolved displacement and momentum thicknesses on the distance-time planes or the ensemble-averaged velocity.

(2) The turbulent spots emerged almost at or slightly upstream of the separation point. This rather early emergence of the turbulent spots could be reasoned by the effect of adverse pressure gradient or the change in curvature as a catalyst of the transition, although much remains to be studied in more detail. The onset of the turbulent spots onset slightly depended on the flow conditions such as Reynolds number or Strouhal number.

(3) The wake generated from the bar moving upwards did not make an explicit contribution to the suppression of the separation bubble. This was partially confirmed by the numerical simulation. On the contrary, the wake-induced turbulence spots and the following calmed region suppressed the separation bubble. The wake-affected separation bubble did not show quick recovery to the state of no wake condition after the wake passage. One possible explanation on this phenomenon was “negative-jet effect” of the upstream wake interacting with the leading edge of the model.

(4) Wake-induced turbulence spots and calmed region were not clearly observed in the case when the wake-generating bar moved downwards.

Acknowledgements

The part of this work was conducted under the financial support from the Ministry of Education and Science as Grants-in-Aid for Scientific Research. The authors are indebted to invaluable supports from Mr. F. Saito of Iwate University.

References

(1) Halstead, D.E., Wisler, D.C., Okiishi, T.H., Walker, G.J., Hodson, H.P. and Shin, H.-W., Boundary Layer Development in Axial Compressors and Turbines, Part 2 of 4: Compressors, ASME Trans., Journal of Turbomachinery, Vol.119 (1995), pp.426–444.

(2) Halstead, D.E., Wisler, D.C., Okiishi, T.H., Walker, G.J., Hodson, H.P. and Shin, H.-W., Boundary Layer Development in Axial Compressors and Turbines, Part 3 of 4: Low Pressure Turbines, ASME Trans., Journal of Turbomachinery, Vol.119 (1995), pp.225–237.

(3) Cumptsy, N.A., Dong, Y. and Li, Y.S., Compressor Blade Boundary Layers in the Presence of Wakes, ASME Paper 95-GT-443, (1995).
(4) Schulte, V. and Hodson, H.P., Wake-Separation Bubble Interaction in Low Pressure Turbines, AIAA Paper AIAA-94-2931, (1994).
(5) Kaszeta, R.W., Simon, T.W. and Ashpis, D.E., Experimental Investigation of Transition to Turbulence as Affected by Passing Wakes, ASME Paper 2001-GT-0195, (2001).
(6) Paxson, D.E. and Mayle, R.E., Laminar Boundary Layer Interaction with an Unsteady Passing Wake, ASME Paper 90-GT-120, (1990).
(7) Brear, M.J., Hodson, H.P. and Harvey, N.W., Pressure Surface Separations in Low Pressure Turbines: Part 1 of 2-Midspan Behaviour, ASME Paper 2001-GT-0437, (2001).
(8) Funazaki, K. and Kato, Y., Studies on a Blade Leading Edge Separation Bubble Affected by Periodic Wakes: Its Transitional Behavior and Boundary Layer Loss Reduction, ASME Paper GT-2002-30221, (2002).
(9) Ottavy, X., Vilmin, S., Opoka, M., Hodson, H. and Gallimore, S., The Effects of Wake-Passing Unsteadiness over a Highly Loaded Compressor-Like Flat Plate, ASME Paper GT-2002-30354, (2002).
(10) Chun, S. and Sung, J., Influence of Unsteady Wake on a Turbulent Separation Bubble, Experiments in Fluids, Vol.32 (2002), pp.269–279.
(11) Furukawa, M., Yamasaki, M. and Inoue, M., A Zonal Approach for Navier-Stokes Computations of Compressible Cascade Flow Fields Using a TVD Finite Volume Method, ASME Trans., Journal of Turbomachinery, Vol.113, No.4 (1991), pp.573–582.
(12) Chakravarthy, S.R., Relaxation Method for Unfactored Implicit Upwind Schemes, AIAA Paper No.84-0165, (1984).
(13) Anderson, W.K., Thomas, J.L. and van Leer, B., Comparison of Finite Volume Flux Vector Splittings for the Euler Equations, AIAA Journal, Vol.24, No.9 (1986), pp.1453–1460.
(14) Wilcox, D.C., Reassessment of the Scale-Determining Equation of Advanced Turbulence Models, AIAA Journal, Vol.26, No.11 (1988), pp.1299–1310.
(15) Horton, H.P., A Semi-Empirical Theory for the Growth and Bursting of Laminar Separation Bubbles, Aeronautical Research Council, CP-1073, (1968).
(16) Funazaki, K., Kitazawa, T., Koizumi, K. and Tanuma, T., Studies on Wake-Disturbed Boundary Layers under the Influences of Favorable Pressure Gradient and Free-Stream Turbulence-Part I: Experimental Setup and Discussions on Transition Model, ASME Paper 97-GT-52, (1997).
(17) Halstead, D.E., Wisler, D.C., Okiishi, T.H., Walker, G.J., Hodson, H.P. and Shin, H.-W., Boundary Layer Development in Axial Compressors and Turbines, Part 1 of 4: Composite Picture, ASME Trans., Journal of Turbomachinery, Vol.119 (1995), pp.114–127.
(18) Funazaki, K., Harada, Y. and Takahashi, E., Control of Separation Bubble on a Blade Leading Edge by a Stationary bar Wake, ASME Paper 2000-GT-267, (2000).